The kinetics of calcite dissolution and precipitation in geologically relevant situations of karst areas. 1. Open system

Article *in* Chemical Geology · March 1985

DOI: 10.1016/0009-2541(85)90046-4

CITATIONS
385

READS
1,193

2 authors, including:

Dreybrodt Wolfgang
University of Bremen
265 PUBLICATIONS **11,017** CITATIONS

SEE PROFILE

Chemical Geology, 48 (1985) 189—211
Elsevier Science Publishers B.V., Amsterdam — Printed in The Netherlands

THE KINETICS OF CALCITE DISSOLUTION AND PRECIPITATION IN GEOLOGICALLY RELEVANT SITUATIONS OF KARST AREAS
1. Open System

DIETER BUHMANN and WOLFGANG DREYBRODT*

Fachbereich 1, Physik, Universität Bremen, 2800 Bremen 33 (Federal Republic of Germany)

(Received February 17, 1984; revised and accepted August 6, 1984)

Abstract

Buhmann, D. and Dreybrodt, W., 1985. The kinetics of calcite dissolution and precipitation in geologically relevant situations of karst areas, 1. Open system. Chem. Geol., 48: 189—211.

A general theory of dissolution and precipitation rates at $CaCO_3$ surfaces from calcareous solutions in contact with an atmosphere containing CO_2 is presented. The three rate-determining processes, kinetics at the $CaCO_3$ surface, diffusion into the bulk and conversion of CO_2 into HCO_3^- are treated simultaneously. In all cases the dissolution or precipitation rates are given by $R = \alpha([Ca^{2+}]_{eq} - [Ca^{2+}])$, where α is a function of CO_2 pressure, thickness of the water film covering the $CaCO_3$ surface, and temperature. α depends also on the hydrodynamic conditions of flow. Under turbulent flow the rates increase by one order of magnitude, since in comparison to laminar flow diffusion is significantly enhanced by eddies.

We have carried out experiments to measure the time dependence of $[Ca^{2+}]$ in stagnant and turbulently-stirred water films covering $CaCO_3$ surfaces for various temperatures, CO_2 pressures and film thicknesses. From the exponential behaviour of $[Ca^{2+}](t)$ the value of α can be determined. Good agreement with the theoretical predictions is obtained. Furthermore, precipitation rates from supersaturated solutions were measured and found to be in good agreement with the theory.

Our results are summarized in a table and figures, which provide the geologist data from which in all situations, being geologically relevant in karst areas as far as open system is concerned, dissolution and precipitation rates can be derived easily.

1. Introduction

Dissolution processes of $CaCO_3$ in H_2O—CO_2 systems play a most important role in the evolution of karst landscapes in limestone areas. To give reliable answers to problems of karst denudation, cave genesis, the development of different types of karren and other morphologic features in karst landscapes, a detailed knowledge of dissolution kinetics is necessary. We have therefore developed a comprehensive theoretical formulation of calcite dissolution and precipitation rates for a simplified geometric situation, which can be applied to many geological situations. To test its reliability we have carried out experiments which verify the theoretical predictions.

The kinetics of calcite dissolution and

*Author to whom all correspondence should be sent.

0009-2541/85/$03.30

precipitation are determined by three independent processes, which all can be rate determining:

(1) The kinetics of dissolution at the phase boundary between the solvent aqueous system $CaCO_3$—H_2O—CO_2 and the limestone rock.

(2) The kinetics of the conversion of CO_2 to carbonic acid H_2CO_3 (Kern, 1960), which constitutes the aggressive agent in the process of $CaCO_3$ dissolution.

(3) Mass transport of the dissolved species, i.e. Ca^{2+}, HCO_3^-, CO_3^{2-}, CO_2 and H_2CO_3, by diffusion from and to the phase boundaries. A rigorous theory has to take into account simultaneously these processes.

There have been many different theories in the past trying to solve this problem. In a first theory Weyl (1958) approached the problem by assuming that the dissolution processes at the $CaCO_3$ surface are so fast that the solution is in chemical equilibrium with the solid at the boundary layer. The rate processes are then entirely determined by mass transport from the boundary layer into the solution. Further progress was achieved by Curl (1968), who took into account the fact that conversion of physically dissolved CO_2 into the chemical aggressive agent H_2CO_3 is a slow process.

These theories, however, all failed to take into account the mechanisms at the surface of the $CaCO_3$ rock. No significant progress was therefore achieved up to 1978, when Plummer et al. (1978) published a comprehensive investigation of dissolution rates of $CaCO_3$ in stirred H_2O—CO_2 systems. In these experiments the rate processes were investigated under turbulent flow conditions. Furthermore, the ratio of the volume of the solution to the surface of the dissolving crystals was so large that CO_2—H_2CO_3 conversion was not rate limiting. Thus the data of Plummer et al. give exact information on the chemical kinetics of surface-controlled dissolution of $CaCO_3$. Plummer et al. summarize their results in a rate equation (the so-called Plummer—Wigley—Parkhurst equation or PWP equation), which gives the dissolution rate as a function of the activities of the species Ca^{2+}, H^+, HCO_3^- and H_2CO_3 at the $CaCO_3$ surface.

With this work sufficient knowledge of all the above-mentioned three processes determining dissolution in natural systems was then available. Moreover, the data of Plummer et al. (1978) are not only applicable to the problem of $CaCO_3$ dissolution but can also be applied to the problem of calcite precipitation (Plummer et al., 1979; Reddy et al., 1981).

A first approach in combining the effects of surface-controlled dissolution, CO_2—H_2CO_3 conversion and mass transport was published by Dreybrodt (1981a). He calculated dissolution rates for thin films of calcareous solution in contact with $CaCO_3$ surfaces for the case of systems open and closed to a CO_2 atmosphere. Thus he modeled the case of thin water films with laminar or turbulent flow in joints of the rock (closed system) or on rock surfaces open to the atmosphere (open system). With these calculations, though many simplifying assumptions had been made, it was possible to give a comprehensive model for the initial phase of cave genesis. In a second paper, Dreybrodt (1981b) applied the PWP equation to the problem of cave genesis after the state of initiation. The scales of time and length in the development of caves, derived from these calculations, are in agreement with observations. Dreybrodt (1981c) also applied the PWP equation to the problem of deposition of calcite in caves. Taking into account diffusion of CO_2 and the PWP equation, he calculated growth rates of speleothems as stalagmites and wall sinter. The values thus calculated were of the same order of magnitude as those observed in nature. The shortcomings of the work of Dreybrodt are that: (1) the theory contains many simplifications; and (2) no experimental data are supplied to support the theoretical predictions. On the other hand, the agreement between the data calculated for cave development and growth of speleothems and those observed in nature is encouraging.

For this reason we have carried out experiments of calcite dissolution and precipitation for simple geometric conditions for systems open and closed to the CO_2 atmosphere. Furthermore, we have developed a comprehensive theory of calcite dissolution and precipitation fully taking into account mass transport, CO_2—H_2CO_3 conversion and surface reactions. In this paper we report the results for $CaCO_3$—H_2O—CO_2 systems open to the atmosphere. The results for closed systems will be reported in a subsequent paper (Buhmann and Dreybrodt, 1985). In the first part of this paper the theory will be established. The corresponding experiments are described thereafter and it will be shown that agreement between experiment and theory is quite satisfactory.

2. Theory of calcite dissolution

2.1. Formulation of the problem

Many geological situations are characterized by thin water films up to 0.1 cm thickness, flowing on bare rocks in the laminar region. Thicker films show turbulent flow. The surface of the water films is in direct contact with the atmosphere and there is a flow of CO_2 into the solution. These open-system conditions govern the processes of karst denudation and the formation of grykes. If the solution is supersaturated, precipitation of calcite occurs, and formation of cave sinter (stalagmites, flowstone, rimstone dams, etc.) sets in.

If we approximate both laminar and turbulent flow in the y-direction as plug flow with a constant velocity v_y, the mass-transport equation for the stationary case is given (Cess and Shaffer, 1959) by:

$$v_y \frac{\partial c}{\partial y} = D \frac{\partial^2 c}{\partial z^2} \qquad (1a)$$

where c is the concentration of the Ca^{2+} ion; and D is the coefficient of diffusion.

This is analogous to the equation describing the time variation of the concentration in a stagnant film on the calcite surface, namely:

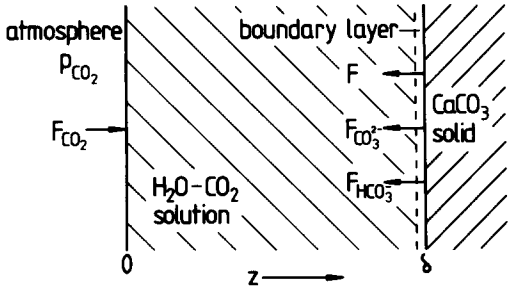

Fig. 1. Model of $CaCO_3$ dissolution in systems open to the atmosphere.

$$\frac{\partial c}{\partial t} = D \frac{\partial^2 c}{\partial z^2} \qquad (1b)$$

The solution of eq. 1a is obtained by replacing t by y/v_y in the solution of eq. 1b (Carslaw and Jaeger, 1959). Thus, in both cases the time variation of the concentration depends only on the time of contact of the solution with the calcite surface.

In the case of turbulent flow one also has to replace the molecular diffusion coefficients of the species involved in mass transport by an effective diffusion coefficient (eddy diffusivity, D_{eff}), which in general is several orders of magnitude higher (Tien, 1959; Bird et al., 1960; Skelland, 1974).

Under these conditions our problem reduces to the simple geometric situation of a water film of thickness δ on a plane calcite surface. Fig. 1 shows this situation. The boundary between atmosphere and fluid is situated at $z = 0$, the boundary between the solid and the solution is at $z = \delta$. During the course of dissolution there is a flux F_{CO_2} of CO_2 into the solution. At $z = \delta$ the flux of Ca^{2+} ions is F. In the case of open systems and for Ca^{2+} concentrations larger than $0.5 \cdot 10^{-4}$ mmol cm^{-3} each molecule of $CaCO_3$ dissolved consumes one molecule of H_2CO_3 for conversion of CO_3^{2-} into HCO_3^-. Therefore, we have the condition that $|F| = |F_{CO_2}|$.

The flow F is given by the PWP equation:

$$F = \kappa_1(H^+) + \kappa_2(H_2CO_3^*) + \kappa_3 - \kappa_4(Ca^{2+})(HCO_3^-) \quad (2)$$

where the quantities in round brackets are the activities of the corresponding species and:

$$(H_2CO_3^*) = (H_2CO_3^0) + (CO_2)$$

The rate constants κ_1, κ_2 and κ_3 are temperature dependent and have been taken from the work of Plummer et al. (1978). The constant κ_4 is dependent on the activity of the aggressive agent $H_2CO_3^0$ in the solution and is given by a curve which fits the experimental data of Plummer et al. for values $P_{CO_2} \leqslant 5 \cdot 10^{-2}$ atm.:

$$\kappa_4 = \exp(-B \ln 10)\ \{K_H(1 + K_0^{-1})/(H_2CO_3^0)\}^{0.611} \quad (3)$$

with

$$B = 3.077 - 0.0146T_C$$

where T_C is the temperature in °C. $(H_2CO_3^0)$ is the activity of carbonic acid present in the solution, i.e. in equilibrium with HCO_3^- and H^+. K_0 and K_H are mass-balance constants as given in eq. 7.

The PWP equation summarizes the effects of three chemical reactions at the calcite surface. These are:

(a) $CaCO_3 + H^+ \rightleftharpoons Ca^{2+} + HCO_3^-$

(b) $CaCO_3 + H_2CO_3^0 \rightleftharpoons Ca^{2+} + 2HCO_3^-$

(c) $CaCO_3 + H_2O \rightleftharpoons Ca^{2+} + HCO_3^- + OH^-$

At pH > 6 reaction (a) is negligible. At pressures $P_{CO_2} < 0.01$ atm. the dominant reaction is reaction (c). The OH^- ion resulting from this reaction is neutralized by protons, which are supplied by the dissociation of carbonic acid. Thus, the conversion of:

$$CO_2 \rightarrow H_2CO_3 \rightarrow H^+ + HCO_3^-$$

plays an important role in the process of dissolution. Two chemical reaction paths effect this conversion. At low pH-values the reaction:

(I) $CO_2 + H_2O \rightleftharpoons H_2CO_3^0 \rightleftharpoons H^+ + HCO_3^-$

is dominant. The first part of this reaction is slow, the second one is so fast that for all cases of interest $H_2CO_3^0$ and HCO_3^- are in equilibrium. At pH > 7 a second reaction becomes important:

(II) $CO_2 + OH^- \rightleftharpoons HCO_3^-$

Thus, the conversion of H_2CO_3 is given (Kern, 1960) by the kinetic equation:

$$\frac{dCO_2}{dt} = -k_1[CO_2] + k_{-1}[H^+][HCO_3^-] - k_2[CO_2][OH^-] + k_{-2}[HCO_3^-] \quad (4a)$$

The quantities in square brackets are concentrations. The numerical values of k_1 and k_2 are taken from Kern (1960) and Welch et al. (1969). k_{-1} and k_{-2} are calculated from k_1 and k_2 using the mass-balance equations (7):

$$k_{-1} = k_1 \gamma_H \gamma_{HCO_3} \frac{K_0}{K_5}$$

$$k_{-2} = k_2 \frac{\gamma_{HCO_3}}{\gamma_{OH}} \frac{K_W K_0}{K_5} \quad (4b)$$

All the other chemical reactions occurring in the solution are fast and equilibrium between the corresponding species can be assumed during the dissolution process. This will be discussed in detail later (see p. 194).

In the next step, diffusion of CO_2 from the atmosphere into the solution and diffusion of Ca^{2+}, CO_3^{2-} and HCO_3^- from the solid into the solution have to be taken into account. This leads to a set of four differential equations, which are well known in theory of diffusion (Bird et al., 1960):

$$-\frac{\partial[CO_2]}{\partial t} + D_{CO_2}\frac{\partial^2[CO_2]}{\partial z^2} = (k_1 + k_2[OH^-]) \times [CO_2] - (k_{-1}[H^+] + k_{-2})[HCO_3^-] = k_+[CO_2] - k_-[HCO_3^-] \quad (5a)$$

$$-\frac{\partial[HCO_3^-]}{\partial t}+D\frac{\partial^2[HCO_3^-]}{\partial z^2}=-(k_1+k_2[OH^-])\times[CO_2]+(k_{-1}[H^+]+k_{-2})[HCO_3^-]+k_{-3}[H^+][CO_3^{2-}]-k_3[HCO_3^-] \quad (5b)$$

$$-\frac{\partial[CO_3^{2-}]}{\partial t}+D\frac{\partial^2[CO_3^{2-}]}{\partial z^2}=k_3[HCO_3^-]-k_{-3}[H^+][CO_3^{2-}] \quad (5c)$$

$$-\frac{\partial[Ca^{2+}]}{\partial t}+D\frac{\partial^2[Ca^{2+}]}{\partial z^2}=0 \quad (5d)$$

The constants k_3 and k_{-3} describe the fast reaction $HCO_3^- \rightleftharpoons H^+ + CO_3^{2-}$ and are introduced for completeness. Eq. 5d is independent of the others, since no reaction of Ca^{2+} with the other species occurs, if one neglects ion pairing. We have assumed the diffusion coefficients D of Ca^{2+}, CO_3^{2-} and HCO_3^- to be of equal magnitude; $D = 0.7D_{CO_2}$.

If ion pairs are not to be neglected, one has to introduce two additional equations of the same type for $CaCO_3^0$ and $CaHCO_3^+$ with the corresponding kinetic terms on the right-hand side. The equation for Ca^{2+} has to be extended by introducing the corresponding kinetic terms on the right-hand side. The same has to be done for eqs. 5b and 5c. If one assumes, however, that the reactions are very fast and equilibrium of these species is maintained, the kinetic terms are small compared to the others and may be neglected in eqs. 5b—5d. Adding then all equations containing Ca^{2+} yields instead of eq. 5d:

$$-\frac{\partial[Ca^{2+}]_T}{\partial t}+D\frac{\partial^2[Ca^{2+}]_T}{\partial z^2}=0 \quad (5d')$$

$[Ca^{2+}]_T$ is then the total Ca^{2+} concentration:

$$[Ca^{2+}]_T=[Ca^{2+}]+[CaCO_3^0]+[CaHCO_3^+] \quad (6)$$

Thus, the introduction of ion pairs leaves eq. 5 unaltered, but the interpretation of eq. 5d is changed in the sense that $[Ca^{2+}]$ has to be replaced by $[Ca^{2+}]_T$.

One important feature of eq. 5 is that CO_2 and HCO_3^- are not in equilibrium with each other, as long as dissolution or precipitation

TABLE I

Temperature dependence of the constants used for the calculations [$T = T_C + 273.16$ (K)]

$\log \kappa_1$	$= 0.198 - 444T^{-1}$	(1)
$\log \kappa_2$	$= 2.84 - 2177T^{-1}$	(1)
$\log \kappa_3$	$= -5.86 - 317T^{-1}$	(1)
$\log K_W$	$= 22.801 - 4787.3T^{-1} - 0.010365T - 7.1321 \log T$	(2)
$\log K_H$	$= 108.3865 - 6919.53T^{-1} + 0.01985076T - 40.45154 \log T + 669365T^{-2}$	(3)
$\log K_2$	$= -107.8871 + 5151.79T^{-1} - 0.03252849T + 38.92561 \log T - 563713.9T^{-2}$	(3)
$\log K_3^{-1}$	$= 1209.120 - 34765.05T^{-1} + 0.31294T - 478.782 \log T$	(3)
$\log K_4^{-1}$	$= -1228.732 + 35512.75T^{-1} - 0.299444T + 485.818 \log T$	(3)
K_5	$= 1.707 \cdot 10^{-4}$	(4)
$\log K_6$	$= -356.3094 + 21834.37T^{-1} - 0.060919964T + 126.8339 \log T - 1684915T^{-2}$	(3)
k_1	$= 10^{-3}[\exp(34.69 - 9252T^{-1})]$	(5)
$\log k_2$	$= 14.072 - 3025T^{-1}$	(6)
D_{CO_2}	$= 10^{-5}(0.56 + 0.058T_C)$; $D = 0.7\ D_{CO_2}$	(7)

References: *1* = Plummer et al. (1978); *2* = Harned and Hamer (1933); *3* = Plummer and Busenberg (1982); *4* = Picknett et al. (1976); *5* = Welch et al. (1969); *6* = Kern (1960); *7* = Landolt and Börnstein (1969).

occurs. However, since all the other reactions are fast we can assume that the species, $H_2CO_3^0$, HCO_3^-, CO_3^{2-}, H^+, OH^-, $CaCO_3^0$, $CaHCO_3^+$ and Ca^{2+}, are practically in equilibrium with each other. Therefore, the mass-balance equations between these species are needed to describe their mutual dependence. They are:

$$(H^+)(OH^-) = K_W(H_2O) \tag{7a}$$

$$(CO_2) = K_H P_{CO_2} \tag{7b}$$

$$(CO_2) = K_0(H_2CO_3^0) \tag{7c}$$

$$(H^+)(HCO_3^-) = K_1(H_2CO_3^*) \tag{7d}$$

$$(H^+)(CO_3^{2-}) = K_2(HCO_3^-) \tag{7e}$$

$$(Ca^{2+})(HCO_3^-) = K_3(CaHCO_3^+) \tag{7f}$$

$$(Ca^{2+})(CO_3^{2-}) = K_4(CaCO_3^0) \tag{7g}$$

$$(H^+)(HCO_3^-) = K_5(H_2CO_3^0) \tag{7h}$$

$$(H^+)(HCO_3^-) = K_6(CO_2)(H_2O) \tag{7i}$$

with

$$(H_2CO_3^*) = (H_2CO_3^0) + (CO_2)$$

where K_H is Henry's constant relating the CO_2 pressure P_{CO_2} of the surrounding atmosphere to the activity of CO_2 dissolved in the solution. Table I gives a survey of the numerical temperature dependence for all constants used in our calculation. The constants K_0 and K_1 are calculated by the relations:

$$\left.\begin{aligned} K_0 &= K_5/K_6 \\ K_1 &= K_5K_6/(K_5 + K_6) \end{aligned}\right| \tag{8}$$

2.2. Calculation of the dissolution rates

To solve the differential equations (5), we note that eq. 5d is independent of eqs. 5a—5c and can therefore be treated first. The boundary conditions for the Ca^{2+} species are:

$$\left.\begin{aligned} -D\,\frac{\partial[Ca^{2+}]}{\partial z/\delta} &= F \\ -D\,\frac{\partial[Ca^{2+}]}{\partial z/0} &= 0 \end{aligned}\right| \tag{9}$$

The flux F is given by the PWP equation (2) and depends on the values of:

$$[Ca^{2+}]_\delta = [Ca^{2+}](\delta)$$

$$[HCO_3^-]_\delta = [HCO_3^-](\delta)$$

and

$$[H^+]_\delta = [H^+](\delta)$$

at the surface of the solid. As long as no equilibrium between the solid and the fluid is achieved, these values are time dependent.

If we assume that dissolution proceeds so slowly that during a given small time interval Δt the composition of the solution remains practically constant, we have the situation of mass transfer with prescribed constant flux F into the solution. In this case the solution of eq. 5d with boundary conditions (9) is given by Carslaw and Jaeger (1959) as:

$$[Ca^{2+}](z) = \left\{ \frac{Ft}{\delta} + \frac{F\delta}{D}\left(\frac{3z^2 - \delta^2}{6\delta^2}\right) - \frac{F\delta}{3D} \right.$$

$$\left. + [Ca^{2+}]_\delta \left\{ -\frac{F\delta}{D} \sum \frac{2(-1)^n}{n^2\pi^2} \right.\right.$$

$$\left.\left. \times \exp\left(-\frac{Dn^2\pi^2}{\delta^2}\, t\right) \cos\left(\frac{n\pi z}{\delta}\right) \right. \right. \tag{10}$$

$[Ca^{2+}]_\delta$ is the concentration at $z = \delta$, at time $t = 0$. The exponentials in expression (10) decay with the time constant $T_D = \delta^2/D\pi^2$. Thus, if the decay time, τ, for the solution to reach equilibrium is large, i.e. $T_D \ll \tau$, the concentration profile $[Ca^{2+}](z)$ can be written:

$$[Ca^{2+}](z) = \frac{Ft}{\delta} + \frac{F\delta}{D}\left(\frac{3z^2 - \delta^2}{6\delta^2}\right) - \frac{F\delta}{3D}$$

$$+ [Ca^{2+}]_\delta \tag{10a}$$

As we will see later (p.205) the experiments show that during the dissolution process equilibrium is achieved exponentially with a time constant in the order of $\tau \approx 10^4$ s. The decay time T_D is 10^3 s for $\delta = 0.3$ cm. Thus, for geologically relevant values of $\delta < 0.3$ cm we can treat the problem as quasi-stationary with solution (10a) for eq. 5d.

To solve the coupled eqs. 5a—5c we use a method proposed by Quinn and Otto (1971).

Adding eqs. 5a—5c leads to:

$$\frac{\partial[CO_2]}{\partial t} + \frac{\partial[HCO_3^-]}{\partial t} + \frac{\partial[CO_3^{2-}]}{\partial t} = D_{CO_2}\frac{\partial^2[CO_2]}{\partial z^2} + D\frac{\partial^2[HCO_3^-]}{\partial z^2} + D\frac{\partial^2[CO_3^{2-}]}{\partial z^2} \quad (11)$$

In the quasi-stationary approximation, we have:

$$\left.\begin{aligned}\frac{\partial[HCO_3^-]}{\partial t} + \frac{\partial[CO_3^{2-}]}{\partial t} &= \frac{F_{HCO_3^-}}{\delta} + \frac{F_{CO_3^{2-}}}{\delta} + \frac{F}{\delta}\\ \frac{\partial[CO_2]}{\partial t} &= 0\end{aligned}\right| \quad (12)$$

where $F_{CO_3^{2-}}$ and $F_{HCO_3^-}$ are the fluxes of the corresponding species from the surface into the solution. The term F/δ arises from the fact that for each Ca^{2+} ion one molecule of CO_2 is converted into HCO_3^-. In open-system conditions within our approximation $\partial[CO_2]/\partial t = 0$.

Furthermore, we have the condition:

$$F_{HCO_3^-} + F_{CO_3^{2-}} = F \quad (13)$$

since each dissolved Ca^{2+} ion releases one C atom. With these conditions we obtain:

$$D_{CO_2}\frac{\partial^2[CO_2]}{\partial z^2} + D\frac{\partial^2[HCO_3^-]}{\partial z^2} + D\frac{\partial^2[CO_3^{2-}]}{\partial z^2} = \frac{2F}{\delta} \quad (14)$$

Integration yields:

$$\frac{2F}{\delta}z + C_1 = D_{CO_2}\frac{\partial[CO_2]}{\partial z} + D\frac{\partial[HCO_3^-]}{\partial z} + D\frac{\partial[CO_3^{2-}]}{\partial z} \quad (15)$$

The integration constant C_1 is determined by the boundary conditions at $z = 0$. These are:

$$\left.\begin{aligned}-D_{CO_2}\frac{\partial[CO_2]}{\partial z} &= -F_{CO_2} = F\\ \frac{\partial[HCO_3^-]}{\partial z} &= \frac{\partial[CO_3^{2-}]}{\partial z} = 0\end{aligned}\right| \quad (16)$$

which yields $C_1 = -F$.

Second integration of eq. 15 yields:

$$\frac{F}{\delta}z^2 - Fz + C_2 = D_{CO_2}[CO_2] + D[HCO_3^-] + D[CO_3^{2-}] \quad (17)$$

The integration constant C_2 is determined from the concentrations $[\cdot]$ at $z = \delta$. Finally, we obtain:

$$\frac{F}{\delta}z^2 - Fz + D_{CO_2}[CO_2]_\delta + D[HCO_3^-]_\delta + D[CO_3^{2-}]_\delta = D_{CO_2}[CO_2] + D[HCO_3^-] + D[CO_3^{2-}] \quad (18)$$

To solve eq. 5a, we have to express $[HCO_3^-]$ as a function of $[CO_2]$. This is achieved by using the equation of electroneutrality (neglecting ion pairs):

$$2[Ca^{2+}] + [H^+] = [HCO_3^-] + 2[CO_3^{2-}] + [OH^-] \quad (19)$$

and inserting the mass-balance equations (7a) and (7e). This gives a quadratic equation for $[H^+]$ with the solution:

$$[H^+] = -\tfrac{1}{2}(2[Ca^{2+}] - [HCO_3^-]) + \left\{\tfrac{1}{4}(2[Ca^{2+}] - [HCO_3^-])^2 + \frac{K_w}{\gamma_H\gamma_{OH}} + \frac{2K_2\gamma_{HCO_3}}{\gamma_H\gamma_{CO_3}}[HCO_3^-]\right\}^{1/2} \quad (20)$$

From eq. 20 the concentration $[CO_3^{2-}]$ is calculated as a function of $[HCO_3^-]$ by inserting eq. 20 into eq. 7e.

Inserting $[CO_3^{2-}]$ into eq. 18 yields a cubic relation for $[HCO_3^-]$ as a function of $[Ca^{2+}]$ and $[CO_2]$:

$$L[HCO_3^-]^3 + M[HCO_3^-]^2 + N[HCO_3^-] + P = 0 \quad (21)$$

with

$$L = K_2\frac{\gamma_{HCO_3}}{\gamma_H\gamma_{CO_3}}$$

$$M = \frac{K_w}{\gamma_H\gamma_{OH}} - L^2 + 3BL + 2L[Ca^{2+}]$$

$$N = 2B\left(\frac{K_w}{\gamma_H\gamma_{OH}} + L[Ca^{2+}] + BL\right)$$

$$P = B^2\frac{K_w}{\gamma_H\gamma_{OH}}$$

and

$$B = \frac{1}{D}\left\{-\frac{F}{\delta}z^2 + Fz - D_{CO_2}([CO_2]_\delta - [CO_2]) - D[CO_3^{2-}]_\delta - D[HCO_3^-]_\delta\right\}$$

If the ion pairs $CaHCO_3^+$ and $CaCO_3^0$ are included, the equation of electroneutrality has to be changed by introducing $CaHCO_3^+$. Using then eqs. 5d′ and 6 instead of eq. 5d for the Ca-containing species one obtains similar equations, which are somewhat more complicated. Our calculations have shown that the introduction of ion pairs changes the results only by less than 3%. Therefore for clarity of presentation, we neglect ion pairs without loss of general validity of our theory.

The ionic activity coefficients γ in all equations were computed by using modified Debye—Hückel theory (cf. Plummer and Busenberg, 1982). The ionic strength has been taken as:

$$I = 3[Ca^{2+}]_{av} \qquad (22)$$

where $[Ca^{2+}]_{av}$ is the average value of $[Ca^{2+}](z)$ taken from $z = 0$ to $z = \delta$. The real value of I is only slightly smaller than the above given value and does not change the calculations in any way.

By using eqs. 7a, 7e, 18, 20 and 21 and the solution of the differential equation (5d) for $[Ca^{2+}]$, the quantities $[HCO_3^-]$, $[H^+]$ and $[OH^-]$ in the differential equation (5a), which describes $[CO_2](z)$, can be expressed as functions of $[CO_2](z)$ and z. Now eq. (5a) can be solved by a Runge—Kutta procedure (Kamke, 1967). Fig. 2 gives a simplified flow diagram for our calculations.

We start with fixed values of temperature, film thickness δ and Ca^{2+} concentration $[Ca^{2+}]_\delta$. We assume a realistic value of $[HCO_3^-]_\delta$. From this value, $[H^+]_\delta$ and $[H_2CO_3^*]_\delta$ in equilibrium

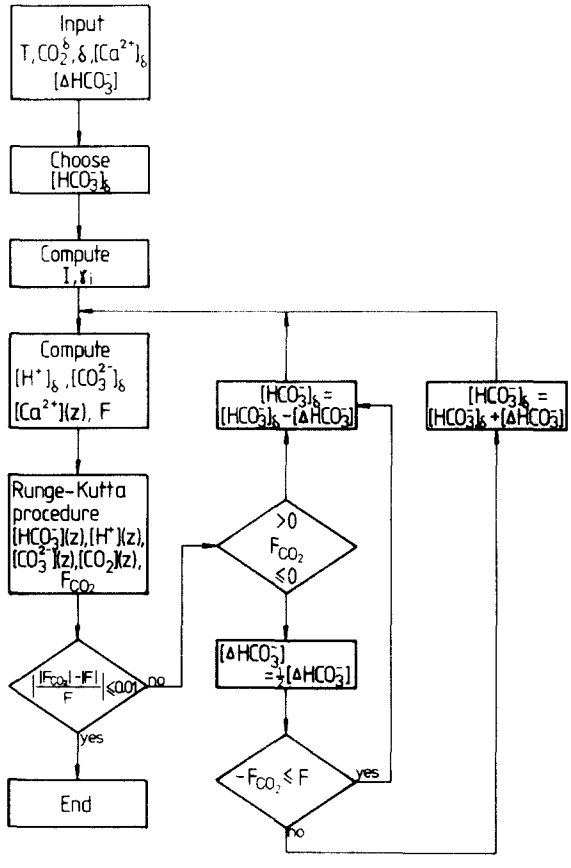

Fig. 2. Flow diagram for the numerical calculations.

with $[H^+]_\delta$ and $[HCO_3^-]_\delta$ are calculated. With these data the flux F of $[Ca^{2+}]$ is obtained by the PWP equation (2) and eq. 3. Now $[Ca^{2+}]\cdot(z)$ can be computed, eq. 10a.

With these data we start the Runge—Kutta procedure at $z = \delta$ for the equation of $[CO_2]$, eq. 5a. The boundary condition is:

$$\frac{\partial[CO_2]}{\partial z/\delta} = 0$$

and for $[CO_2]_\delta$ we choose a realistic value, which is close to $[CO_2](0) = K_H P_{CO_2}$ but somewhat smaller. The Runge—Kutta procedure yields $[CO_2](z)$ and the flux:

$$F_{CO_2} = D_{CO_2}\frac{\partial[CO_2]}{\partial z/0}$$

from the surrounding atmosphere into the fluid.

The crucial condition for the correct solution is that the flux F_{CO_2} into the fluid and the flux F of Ca^{2+} from the solid are of equal magnitude, i.e. $|F_{CO_2}| = |F|$. To achieve this condition the arbitrarily chosen value of $[HCO_3^-]_\delta$ is changed by $[\Delta HCO_3^-]$ by using an iterative half-step procedure until $|F_{CO_2}|$ and $|F|$ differ by less than 1%. Once this is obtained, the profiles $[CO_2](z)$, $[HCO_3^-](z)$, $[H^+](z)$, $[CO_3^{2-}](z)$ and $[Ca^{2+}](z)$ are printed out. The value of $[CO_2](0)$ is then compared to the value $[CO_2] = K_H P_{CO_2}$ and $[CO_2]_\delta$ is changed until $[CO_2]_0$ and $K_H P_{CO_2}$ differ by less than 1%.

As a final remark to this section, we want to stress that this theory is also applicable in the case of calcite precipitation, the only difference being that the signs of F and F_{CO_2} are reversed, since the flux of Ca^{2+} is now directed towards the $CaCO_3$ surface and CO_2 is released into the surrounding atmosphere.

2.3. *Results*

Fig. 3a shows the dissolution rates as a function of the Ca^{2+} concentration averaged from $z = 0$ to $z = \delta$, since this is the value which can be measured experimentally. $[Ca^{2+}]_{av}$ is related to $[Ca^{2+}]_\delta$ by:

$$[Ca^{2+}]_{av} = [Ca^{2+}]_\delta - F\delta/3D \qquad (23)$$

For Ca^{2+} concentrations $[Ca^{2+}] \geqslant 0.2[Ca^{2+}]_{eq}$ the curves can be reasonably well approximated by a linear relation:

$$F = \alpha\{[Ca^{2+}]_{eq} - [Ca^{2+}]\} \qquad (24)$$

where $[Ca^{2+}]_{eq}$ is the concentration at saturation and α is a function of δ, P_{CO_2} and temperature. For $\delta \leqslant 0.003$ cm, α increases nearly linearly with δ. This is the region where conversion of CO_2 into $H_2CO_3^0$ is rate determining. At $\delta \approx 0.03$ cm a threshold is reached and above $\delta = 0.05$ cm the dissolution rate decreases. In this region mass-transport effects become significant. For $[Ca^{2+}] \leqslant 0.2[Ca^{2+}]_{eq}$ a steep increase in the rate curves appears. We will not treat this effect further, since most of the dissolution proceeds in the region of the smaller slopes and our experiments provide data in this region.

The upper curve in Fig. 3a was calculated with $\delta = 1$ cm and with a large value of D_{CO_2} which is increased by a factor of 10^4 from its

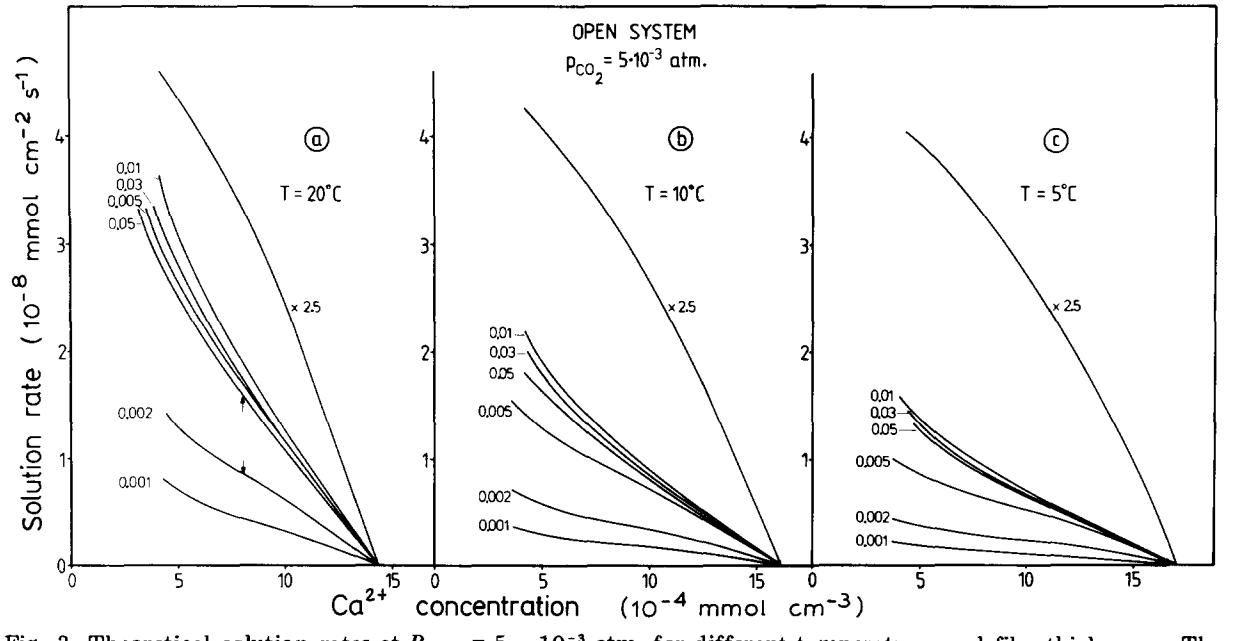

Fig. 3. Theoretical solution rates at $P_{CO_2} = 5 \cdot 10^{-3}$ atm. for different temperatures and film thicknesses. The *number on the solid lines* gives the film thickness δ in cm. The uppermost curves must be multiplied by a factor of 2.5 as indicated in the figure. The *arrows* in (a) indicate the situations for which the concentration profiles in Fig. 4 are calculated.

real value. This simulates turbulent flow, and the rates are determined entirely by surface-controlled processes, i.e. the PWP equation (2). We will discuss this in detail later (p. 202). It is remarkable to see that in this case the rates increase by about one order of magnitude. This clearly proves for the first time the postulate of a hydraulic jump which has been proposed by White and Longyear (1962) as an important feature in the genesis of caves.

Fig. 3b and c shows the dissolution rates at $P_{CO_2} = 5 \cdot 10^{-3}$ atm. for temperatures of 10° and 5°C. Clearly a change in $\alpha(\delta, T, P_{CO_2})$ is observed. The α increase with temperature. The reason for this change is the temperature dependence of the kinetic constants of the $CO_2 \rightarrow H_2CO_3^0$ conversion as is shown in Section 2.4.

Fig. 4 gives the concentration profiles with the parameters of Fig. 3a for $\delta = 0.002$ cm and $\delta = 0.05$ cm. In the case of thin films no concentration profiles build up, especially $[H^+]$ is almost constant over the film. At larger δ-values diffusion profiles develop, showing that mass transport becomes significant. In both cases $[HCO_3^-]$ shows little variation over the fluid film.

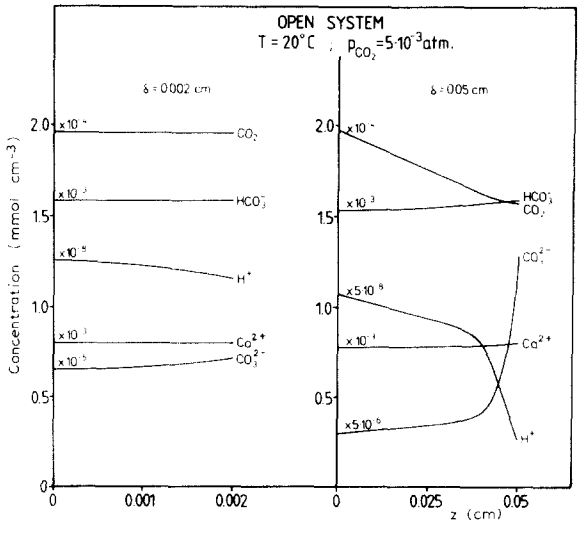

Fig. 4. Concentration profiles of CO_2 and the four most important ions at $[Ca^{2+}]_\delta = 8 \cdot 10^{-4}$ mmol cm^{-3} across water films of 0.002- and 0.05-cm thickness. The concentration scale for the individual species has to be multiplied by the factor given at the corresponding line.

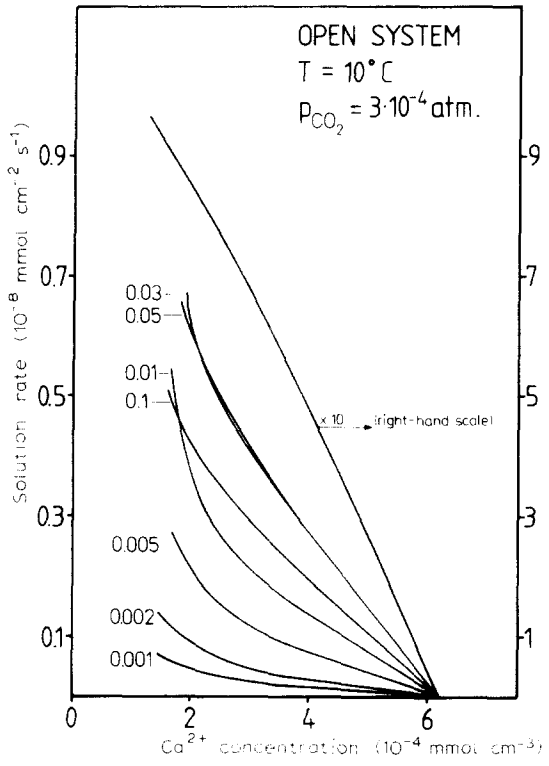

Fig. 5. Theoretical solution rates at $P_{CO_2} = 3 \cdot 10^{-4}$ atm. and $T = 10$°C for various film thicknesses. The *number on the solid curves* gives the film thickness δ in cm. The uppermost curve has to be multiplied by a factor of 10 or to be read by the right-hand scale.

Fig. 5 shows the rates for various values of δ with $P_{CO_2} = 3 \cdot 10^{-4}$ atm. and $T = 10$°C. Here similar features as in Fig. 3 are seen.

To summarize the results we have listed the values of α for various values of temperature, P_{CO_2} and δ in Table II, (a). At small values of δ there is a significant variation of α with δ, showing that CO_2 conversion is the dominant process. With increasing δ-values this variation becomes significantly weaker, indicating that mass transport becomes dominant.

one can obtain diagrams for deposition of $CaCO_3$. In this case the signs of F_{CO_2} and F are reversed with respect to the case of dissolution. The starting calcite solution must be supersaturated.

Fig. 6 gives the results for δ from 0.005 to 0.02 cm at $T = 10°$ and 20°C. The CO_2 partial pressure of the surrounding atmosphere is

TABLE II

Numerical values of $\alpha = \alpha(T,\delta)$ in cm s^{-1} at various partial pressures of CO_2 (in atm.): part (a) for laminar flow; and part (b) for turbulent flow ($D_{eff} = 10^4 D_{CO_2}$). Part (c) gives the calculated Ca^{2+} concentrations at saturation, $[Ca^{2+}]_{eq}$

δ (cm)	T = 5°C			T = 10°C			T = 20°C		
	$3 \cdot 10^{-4}$	$1 \cdot 10^{-3}$	$5 \cdot 10^{-3}$	$3 \cdot 10^{-4}$	$1 \cdot 10^{-3}$	$5 \cdot 10^{-3}$	$3 \cdot 10^{-4}$	$1 \cdot 10^{-3}$	$5 \cdot 10^{-3}$
(a) *Laminar flow*:									
0.001	$4.1 \cdot 10^{-7}$	$6.19 \cdot 10^{-7}$	$1.53 \cdot 10^{-6}$	$7.14 \cdot 10^{-7}$	$1.1 \cdot 10^{-6}$	$2.5 \cdot 10^{-6}$	$2.32 \cdot 10^{-6}$	$3.58 \cdot 10^{-6}$	$6.79 \cdot 10^{-6}$
0.002	$7.6 \cdot 10^{-7}$	$1.34 \cdot 10^{-6}$	$2.94 \cdot 10^{-6}$	$1.35 \cdot 10^{-6}$	$2.33 \cdot 10^{-6}$	$4.67 \cdot 10^{-6}$	$4.07 \cdot 10^{-6}$	$7.5 \cdot 10^{-6}$	$1.36 \cdot 10^{-5}$
0.005	$1.97 \cdot 10^{-6}$	$3.3 \cdot 10^{-6}$	$6.47 \cdot 10^{-6}$	$3.41 \cdot 10^{-6}$	$5.83 \cdot 10^{-6}$	$1.11 \cdot 10^{-5}$	$1.04 \cdot 10^{-5}$	$1.69 \cdot 10^{-5}$	$2.74 \cdot 10^{-5}$
0.01	$3.7 \cdot 10^{-6}$	$6.19 \cdot 10^{-6}$	$1.00 \cdot 10^{-5}$	$6.35 \cdot 10^{-6}$	$1.08 \cdot 10^{-5}$	$1.54 \cdot 10^{-5}$	$1.84 \cdot 10^{-5}$	$2.76 \cdot 10^{-5}$	$3.13 \cdot 10^{-5}$
0.03	$8.03 \cdot 10^{-6}$	$9.79 \cdot 10^{-6}$	$9.69 \cdot 10^{-6}$	$1.29 \cdot 10^{-5}$	$1.61 \cdot 10^{-5}$	$1.47 \cdot 10^{-5}$	$2.91 \cdot 10^{-5}$	$3.29 \cdot 10^{-5}$	$2.87 \cdot 10^{-5}$
0.05	$9.15 \cdot 10^{-6}$	$9.07 \cdot 10^{-6}$	$9.26 \cdot 10^{-6}$	$1.29 \cdot 10^{-5}$	$1.4 \cdot 10^{-5}$	$1.35 \cdot 10^{-5}$	$2.57 \cdot 10^{-5}$	$2.64 \cdot 10^{-5}$	$2.63 \cdot 10^{-5}$
0.1	$6.36 \cdot 10^{-6}$	$6.8 \cdot 10^{-6}$	$8.5 \cdot 10^{-6}$	$9.19 \cdot 10^{-6}$	$1.0 \cdot 10^{-5}$	$1.21 \cdot 10^{-5}$	$1.6 \cdot 10^{-5}$	$1.63 \cdot 10^{-5}$	$2.0 \cdot 10^{-5}$
(b) *Turbulent flow*:									
0.1	$3.3 \cdot 10^{-5}$	$5.2 \cdot 10^{-5}$	$7.25 \cdot 10^{-5}$	$5.7 \cdot 10^{-5}$	$8.0 \cdot 10^{-5}$	$8.3 \cdot 10^{-5}$	$1.35 \cdot 10^{-4}$	$1.47 \cdot 10^{-4}$	$1.1 \cdot 10^{-4}$
0.2	$5.9 \cdot 10^{-5}$	$8.4 \cdot 10^{-5}$	$7.9 \cdot 10^{-5}$	$9.5 \cdot 10^{-5}$	$1.15 \cdot 10^{-4}$	$8.8 \cdot 10^{-5}$	$2.0 \cdot 10^{-4}$	$1.75 \cdot 10^{-4}$	$1.2 \cdot 10^{-4}$
0.5	$1.15 \cdot 10^{-4}$	$1.2 \cdot 10^{-4}$	$8.0 \cdot 10^{-5}$	$1.65 \cdot 10^{-4}$	$1.45 \cdot 10^{-4}$	$9.0 \cdot 10^{-5}$	$2.6 \cdot 10^{-4}$	$1.85 \cdot 10^{-4}$	$1.2 \cdot 10^{-4}$
1.0	$1.6 \cdot 10^{-4}$	$1.35 \cdot 10^{-4}$	$8.0 \cdot 10^{-5}$	$2.06 \cdot 10^{-4}$	$1.5 \cdot 10^{-4}$	$9.0 \cdot 10^{-5}$	$2.85 \cdot 10^{-4}$	$1.9 \cdot 10^{-4}$	$1.2 \cdot 10^{-4}$
$\geqslant 2.0$	$2.0 \cdot 10^{-4}$	$1.35 \cdot 10^{-4}$	$8.0 \cdot 10^{-5}$	$2.4 \cdot 10^{-4}$	$1.5 \cdot 10^{-4}$	$9.0 \cdot 10^{-5}$	$3.0 \cdot 10^{-4}$	$1.9 \cdot 10^{-4}$	$1.2 \cdot 10^{-4}$
(c) *Ca^{2+} concentrations at saturation*:									
$[Ca^{2+}]_{eq}$ (mmol cm^{-3})	$6.75 \cdot 10^{-4}$	$10.0 \cdot 10^{-4}$	$17.0 \cdot 10^{-4}$	$6.3 \cdot 10^{-4}$	$9.3 \cdot 10^{-4}$	$16.2 \cdot 10^{-4}$	$5.6 \cdot 10^{-4}$	$8.3 \cdot 10^{-4}$	$14.3 \cdot 10^{-4}$

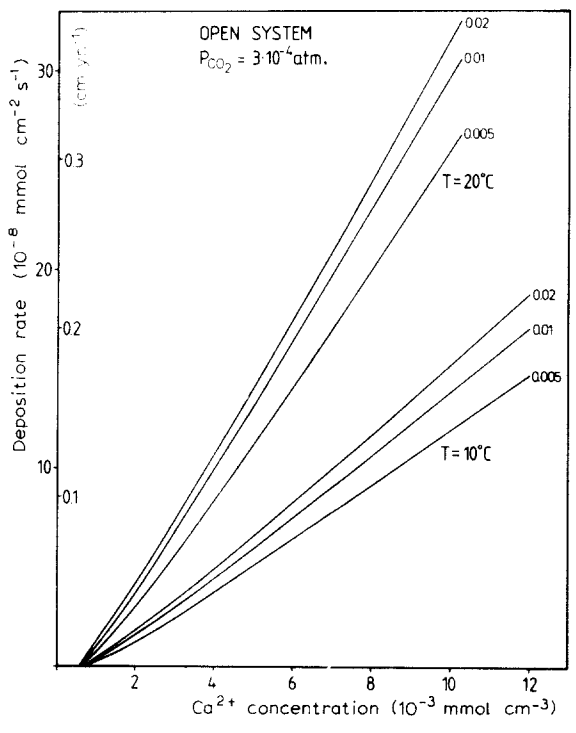

Fig. 6. Theoretical deposition rates at T = 10°C and T = 20°C. The partial pressure of CO_2 in the surrounding atmosphere is 3 • 10^{-4} atm. The *number on the solid curves* gives the film thickness δ in cm.

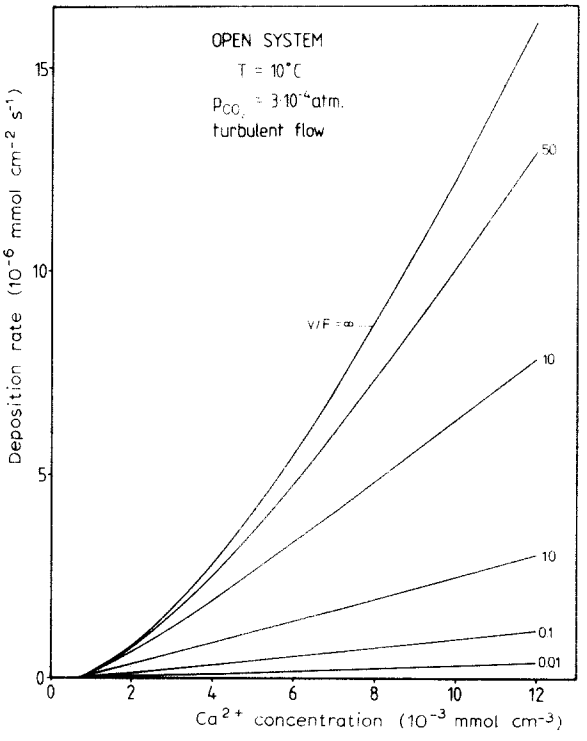

Fig. 7. Theoretical deposition rates under turbulent flow conditions for various film thicknesses δ (*numbers on the solid curves*, in cm). The diffusion coefficients D are assumed to be so high that no concentration gradients build up. The uppermost curve indicates the limit of infinite film thickness which yields the largest possible deposition rates.

$3 \cdot 10^{-4}$ atm. This describes the situation for deposition of cave sinter, such as stalagmites, stalagtites, flow stone and rimstone dams (Dreybrodt, 1980). In the region between 0.005 and 0.02 cm the deposition rates are diffusion controlled. Raising the temperature from 10° to 20°C increases the deposition rates by a factor of ~2. For δ-values below 0.002 cm the deposition shows a similar behaviour to that of the dissolution rates. Since, however, such small film thicknesses are not relevant for the formation of speleothems the results are not shown.

If the calcareous solution flows in a turbulent way ($D_{\text{eff}} \geqslant 10^3 D_{CO_2}$) over the calcite surface, a dramatic increase in deposition rates occurs. Fig. 7 shows this for various values of δ. We can see that the formation of speleothems depends strongly on the prevailing flow conditions. Regular stalagmites usually do not become higher than a few metres and form under stagnant water films on their top. Large stalagmites, which can grow up to several tens of metres and show irregular structures grow under turbulent flow conditions. Rimstone dams also grow under turbulent flow conditions and their shapes can be understood from the data of Fig. 7.

2.4. *Discussion of the results*

To gain some more insight into the physics of the eqs. 5, we tried to find solutions of eqs. 5 leading to closed expressions. One way of doing this is to relax the condition of electroneutrality and use instead the condition of constant $[H^+]$ over the film. This approximation has been used by Hoover and Berkshire (1969) to calculate flux rates of CO_2 into the oceans.

The assumption of a constant pH-value across the water film is justified for $\delta \leqslant 2 \cdot 10^{-2}$ cm and for the case of turbulent flow regime where the diffusion coefficients become large. In the other regimes the rates obtained are larger than those calculated from our previous theory. The expressions, which are obtained in closed form, however, show insight into what happens during dissolution and precipitation and are therefore useful in the discussion of our results.

We use the equation of electroneutrality in the relaxed form:

$$2[Ca^{2+}] = [HCO_3^-] + 2[CO_3^{2-}] \qquad (25)$$

Introducing eq. 25 into eq. 18 we obtain:

$$[HCO_3^-] = \frac{F}{D\delta} z^2 - \frac{2F}{D} z + \frac{F\delta}{D} + 2\frac{D_{CO_2}}{D} \times ([CO_2]_\delta - [CO_2]) + [HCO_3^-]_\delta \qquad (26)$$

We now compute $[H^+]_\delta$ in equilibrium with $[HCO_3^-]_\delta$ by eq. 20 and assume $[H^+](z) = [H^+]_\delta$. Thus, we obtain for eq. 5a:

$$D_{CO_2}\frac{\partial^2[CO_2]}{\partial z^2} = k_{eff}[CO_2] - \kappa - \gamma(z^2/\delta^2 - 2z/\delta) \qquad (27)$$

with the abbreviations:

$$k_{eff} = k_+ + 2\frac{D_{CO_2}}{D}k_-$$

$$\kappa = k_- \left\{ [HCO_3^-]_\delta + 2\frac{D_{CO_2}}{D}[CO_2]_\delta + \frac{F\delta}{D} \right\}$$

$$\gamma = k_- \frac{F\delta}{D}$$

$$k_+ = k_1 + k_2 \frac{K_W}{[H^+]_\delta \gamma_H \gamma_{OH}}$$

$$k_- = k_{-1}[H^+]_\delta + k_{-2}$$

Due to the assumption $[H^+] = [H^+]_\delta$ the coefficients k_+ and k_- become constant and eq. 27 can be solved in closed form. The solution is:

$$[CO_2] = A_1 \cosh\left(\frac{z}{\lambda}\right) + A_2 \sinh\left(\frac{z}{\lambda}\right) + \frac{\kappa}{k_{eff}} + \frac{2D_{CO_2}\gamma}{k_{eff}^2\delta^2} + \frac{\gamma}{k_{eff}}\left(\frac{z^2}{\delta^2} - \frac{2z}{\delta}\right) \qquad (28)$$

where λ is the diffusion length, $\lambda = (D_{CO_2}/k_{eff})^{1/2}$. The constants A_1 and A_2 are determined from the boundary conditions:

$$[CO_2](0) = c_P = K_H P_{CO_2} \qquad \text{at} \qquad z = 0$$

and

$$\frac{\partial[CO_2]}{\partial z/\delta} = 0 \qquad \text{at} \qquad z = \delta$$

giving:

$$\left.\begin{aligned} A_1 &= [CO_2]_0 - \frac{\kappa}{k_{eff}} - \frac{2D_{CO_2}\gamma}{k_{eff}^2\delta^2} \\ A_2 &= -A_1 \tanh(\delta/\lambda) \end{aligned}\right| \qquad (29)$$

The flux F_{CO_2} is now calculated from:

$$D_{CO_2}\frac{\partial[CO_2]}{\partial z/0} = F_{CO_2} \qquad \text{at} \qquad z = 0$$

The result is:

$$F_{CO_2} = \left[D_{CO_2} \left\{ [CO_2]_0 - \frac{k_-}{k_{eff}} \left([HCO_3^-]_\delta + 2\frac{D_{CO_2}}{D}[CO_2]_\delta \right) \right\} - D_{CO_2}\frac{F\delta}{D}\frac{k_-}{k_{eff}} \times \left(1 + \frac{2D_{CO_2}}{k_{eff}\delta^2}\right) \right] \left(\frac{k_{eff}}{D_{CO_2}}\right)^{1/2} \times \tanh\left\{ \left(\frac{k_{eff}}{D_{CO_2}}\right)^{1/2} \delta \right\} + F\frac{2D_{CO_2}}{D}\frac{k_-}{k_{eff}} \qquad (30)$$

The value $[CO_2]_\delta$ is derived from eq. 28:

$$[CO_2]_\delta = \left\{ \frac{1}{\cosh(\delta/\lambda)}[CO_2]_0 + \left(1 - \frac{1}{\cosh(\delta/\lambda)}\right)\left(\frac{k_-}{k_{eff}}[HCO_3^-]_\delta + \frac{k_-}{k_{eff}}\frac{F\delta}{D}\right) + \left(1 - \frac{1}{\cosh(\delta/\lambda)}\right)\frac{2D_{CO_2}\gamma}{k_{eff}^2\delta^2} - \frac{\gamma}{k_{eff}} \right\} \left\{ 1 - \left(1 - \frac{1}{\cosh(\delta/\lambda)}\right) \times \frac{2D_{CO_2}}{D}\frac{k_-}{k_{eff}} \right\}^{-1} \qquad (31)$$

The condition for the correct solution is again $|F_{CO_2}| = |F|$ and the numerical calculation proceeds in a similar way to that described

previously (cf. discussion of Fig. 2 on p. 196).

We use eq. 30 to discuss the different limiting cases for dissolution. For $\delta \ll \lambda$, $\tanh(\delta/\lambda)$ can be approximated by its argument. Taking into account the numerical values of D_{CO_2}, k_- and k_{eff}, neglecting terms proportional to δ^2 and expressing $[CO_2]_\delta$ by eq. 26 yields after some algebra:

$$|F_{CO_2}| = \delta([CO_2]_0 k_+ - k_-[HCO_3^-]_0) = |F| \quad (32)$$

Eq. 32 expresses the amount of CO_2 which is converted into HCO_3^-. At small δ this amount is limited by the volume of the solution and the temperature dependence of the rates is determined by that of k_+ and k_-. Thus, conversion of CO_2 is rate limiting. This can also be seen by the fact that, if we assume k_+ and k_- to be very large, i.e. we relax the condition of slow conversion, the calculations yield F-values which are determined entirely by the PWP equation (2) for a solution where all species, CO_2, HCO_3^-, CO_3^{2-}, H^+ and OH^-, are in equilibrium with each other.

In the case of $\delta > \lambda$ the behaviour of the dissolution rates is governed by the function $\tanh(\delta/\lambda)$, which approaches unity for large δ. Thus, F reaches a limit which is determined by both diffusion and CO_2 conversion, since $\lambda = (D_{CO_2}/k_{eff})^{1/2}$. The fact that with values of $\delta > 0.03$ cm a decrease of the rates occurs, stems from this limit of F and from diffusion of Ca^{2+}, since $[Ca^{2+}]_{av}$ is related to $[Ca^{2+}]_\delta$ by eq. 23, which shifts the average Ca^{2+} concentration towards smaller values.

The case of turbulent flow can be understood as well. In this case a diffusion boundary layer of thickness δ_d is existing which, in all geologically relevant situations, is in the order of several 10^{-3} cm (Dreybrodt, 1981b). Outside of this layer a turbulent core exists, where the effective diffusivity (eddy diffusivity) is $\sim 10^4 D_{CO_2}$ (Skelland, 1974). Thus mass transport is controlled by mixed kinetics (Rickard and Sjöberg, 1983).

If we approximate the chemically controlled surface processes by:

$$F_c = \alpha_c([Ca^{2+}]_{eq} - [Ca^{2+}]_s) \quad (33)$$

and diffusional mass transport by:

$$F_d = \alpha_d([Ca^{2+}]_s - [Ca^{2+}]) \quad (34)$$

with

$$\alpha_d = D/\delta_d$$

where $[Ca^{2+}]$ is the concentration in the turbulent core and $[Ca^{2+}]_s$ the concentration at the calcite surface, we can write (Rickard and Sjöberg, 1983):

$$F = \alpha([Ca^{2+}]_{eq} - [Ca^{2+}]) \quad (35)$$

with

$$\alpha = \alpha_d\alpha_c/(\alpha_d + \alpha_c)$$

The maximum value of α_c is obtained when the concentrations of all species at the surface are equal to that in the bulk. From our calculations we obtain $\alpha_c \approx 10^{-4}$ cm s^{-1} [see Table II, (b)]. α_d is in the order of 10^{-2} cm s^{-1}. Thus $\alpha_d \gg \alpha_c$ and we can set $\alpha = \alpha_c$. In that case the rate is chemically controlled and the influence of the boundary layer may be neglected. Therefore, we can replace the molecular diffusion coefficients D by the effective diffusion coefficients D_{eff} in our theory to simulate turbulent flow.

Increasing the diffusion coefficients by a factor of n increases λ by a factor of $n^{1/2}$. Thus, diffusion as the rate-limiting process is eliminated and eq. 32 must be applied for $\delta \leqslant 0.3\lambda n^{1/2}$. For $n \geqslant 10^3$ these are values of $\delta \leqslant 0.9$ cm. Then CO_2 conversion is no longer rate limiting at sufficiently high pressure, $P_{CO_2} \geqslant 10^{-3}$ atm., and the surface-controlled processes determine the rates.

This can be easily shown by the following considerations. If CO_2 conversion is no longer rate limiting, HCO_3^- and CO_2 are almost in equilibrium with each other. The rates then can be calculated from the PWP equation (2), if all ionic species in equilibrium at a given concentration of $[Ca^{2+}]$ and $[CO_2] = P_{CO_2}K_H$ are known. These equilibrium concentrations can be derived by first expressing the concentrations $[HCO_3^-]$ and $[CO_3^{2-}]$ in terms of P_{CO_2} and $[H^+]$ through the mass-balance

equations:

$$\left.\begin{aligned}[HCO_3^-] &= \frac{[H_2CO_3^*]\,K_1}{\gamma_H\,\gamma_{CO_2}\,[H^+]} \\ &= \frac{(1+K_0^{-1})P_{CO_2}K_HK_1}{\gamma_H\,\gamma_{CO_2}\,[H^+]} \\ [CO_3^{2-}] &= \frac{\gamma_{HCO_3}[HCO_3^-]K_2}{\gamma_H\,[H^+]} \\ &= \frac{\gamma_{HCO_3}(1+K_0^{-1})P_{CO_2}K_HK_1K_2}{\gamma_H^2\,\gamma_{CO_2}\,[H^+]^2}\end{aligned}\right| \quad (36)$$

Substituting into the equation of electroneutrality (19) yields an equation which can be solved for $[H^+]$. From this $[H_2CO_3^*]$, $[HCO_3^-]$ and $[H^+]$ at the surface are known (eq. 36) and the rates can be computed from the PWP equation (2).

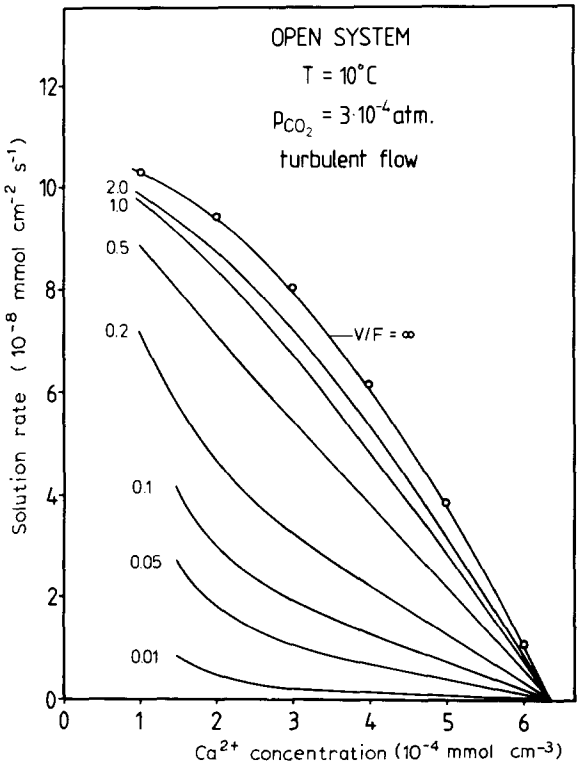

Fig. 8. Theoretical solution rates under turbulent flow conditions for various film thicknesses δ. The *number on the solid curves* gives δ in cm. The uppermost curve indicates the limit of infinite film thickness and is calculated for δ = 10 cm. The *open circles* are calculated from equilibrium theory as described in the text.

These values are in perfect agreement with those calculated from our exact theory, provided n and δ are chosen to be sufficiently high, i.e. $n = 10^4$ and $\delta > 2$ cm for all cases of interest. Fig. 8 shows these results ($n = 10^4$, $P_{CO_2} = 3 \cdot 10^{-4}$ atm., T = 10°C) for various values of δ. The uppermost curve has been calculated for δ = 10 cm from our kinetic theory. The open circles are the values obtained from the equilibrium calculations described above. For small values of δ, CO_2 conversion is rate determining. With increasing values of δ the rates increase until a limit is set by the surface-controlled dissolution.

To summarize our results for the simulation of turbulent flow, we have listed in Table II, (b) the values of α for various film thicknesses, P_{CO_2} and temperature.

It should be noted at this point that the theoretical approach of Dreybrodt (1981a, 1982), who considered the effect of CO_2 conversion for dissolution in open and closed systems, is correct for this limit of high effective diffusion coefficients in turbulent flow. The values calculated by Dreybrodt (1982, fig. 4), are in perfect agreement to those given in Fig. 8 of this paper.

3. Experimental

3.1. Experimental method

To prove our theoretical results we proceeded as follows. We measured the time dependence of the average Ca^{2+} concentration of a water film with thickness δ covering a plane calcite surface and in contact with an atmosphere of known CO_2 pressure. Since the dissolution rates are approximately a linear function of the average Ca^{2+} concentration, we have:

$$\frac{d[Ca^{2+}]_{av}}{dt} = \frac{F}{\delta} = \frac{\alpha}{\delta}([Ca^{2+}]_{eq} - [Ca^{2+}]_{av}) \quad (37)$$

Thus we obtain:

$$[Ca^{2+}]_{av}(t) = \left\{1 - \exp\left(-\frac{\alpha}{\delta}t\right)\right\} [Ca^{2+}]_{eq} \quad (38)$$

or

$$[Ca^{2+}]_{eq} - [Ca^{2+}]_{av}(t) = [Ca^{2+}]_{eq} \exp\left(-\frac{\alpha}{\delta}t\right)$$

if the concentration is zero at $t = 0$.

From the exponential approach of $[Ca^{2+}]_{av}$ (t) to equilibrium, the time constant $\tau = \delta/\alpha$ can be measured and from this α can be determined.

For the purpose of our measurements constant temperature and defined CO_2 pressure of the surrounding atmosphere are required. Therefore $CaCO_3$ specimens were placed in a desiccator, which could be evacuated. The desiccator was placed in a temperature-regulated (±0.5°C) thermostatic chamber. Measurements were performed at 10° and 20°C.

$CaCO_3$ specimens of ~50-cm² surface were cut and surface-polished from white crystalline marble (Carrara Marble) and from pure limestone (Sollnhofen, F.R.G.). One series of measurements was performed on the cleavage plane of a large single crystal of $CaCO_3$. The marble and limestone surfaces were treated with dilute HCl before the first experiment. The surface of the $CaCO_3$ crystal was used untreated.

The specimens were surrounded by Teflon®, and double-distilled water of known volume was brought onto the specimen and evenly distributed over the surface. The specimen was then placed in the desiccator, which was evacuated and filled with an atmosphere of known CO_2 content.

To avoid errors due to evaporation of water from the surface, the bottom of the desiccator was covered with water. After the specimen had rested for a time t the water was picked up with a pipette and stored in a flask containing 0.1 ml of concentrated HCl, to avoid precipitation of $CaCO_3$ after outgassing of CO_2. The Ca^{2+} concentration was measured by atomic absorption spectroscopy. The atmosphere of known CO_2 content was purchased as artificial air (80% N_2—20% O_2) with partial CO_2 pressures of $3 \cdot 10^{-4}$ and $5 \cdot 10^{-3}$ atm.

3.2. *Experimental results*

Fig. 9a shows the measured time dependence of $[Ca^{2+}]$ for T = 10°C and P_{CO_2} = $5 \cdot 10^{-3}$ atm. and δ = 0.1 cm. A semi-logarithmic plot of $[Ca^{2+}]_{eq} - [Ca^{2+}](t)$ is shown in Fig. 9b. The data points lie on a straight line, from which the time constant τ and thus α can be derived. At $t = 0$ the semi-logarithmic plot should intersect the $[Ca^{2+}]$-axis at $[Ca^{2+}]_{eq}$. This, however, is not observed ex-

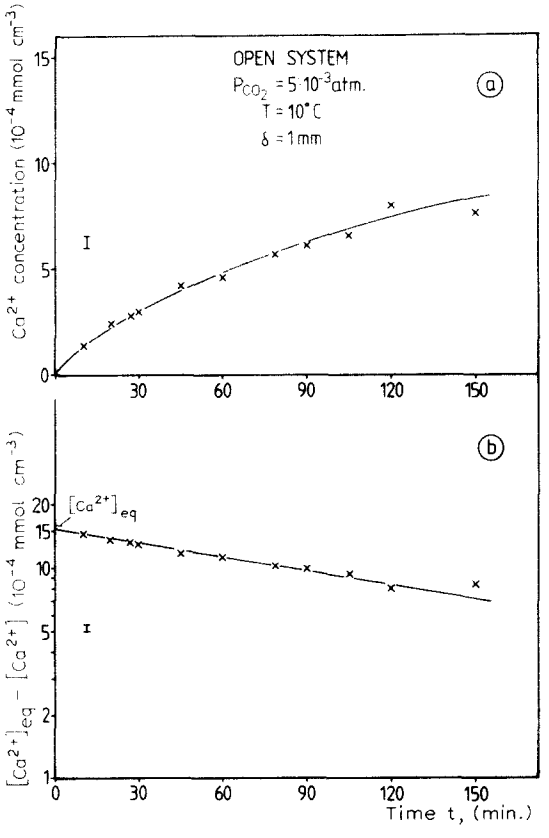

Fig. 9. Experimental results of $CaCO_3$ dissolution at T = 10°C, P_{CO_2} = $5 \cdot 10^{-3}$ atm. and δ = 0.1 cm with time dependence of the Ca^{2+} concentration in a stagnant film of solution.

perimentally. The reason for this behaviour is that at low Ca^{2+} concentrations the dissolution curves rise more steeply than for $[Ca^{2+}] \geqslant 3 \cdot 10^{-4}$ mmol cm^{-3}. In a series of experiments we have measured τ as a function of δ. The δ-values range from 0.03 to 0.15 cm. Lower δ-values could not be investigated, since for smaller film thicknesses an even distribution of the water film over the calcite surface could not be obtained.

Fig. 10 shows the results for τ at $P_{CO_2} = 5 \cdot 10^{-3}$ atm. for temperatures of 10° and 20°C. If this is compared to the theoretical predictions by using the relation $\tau = \delta/\alpha$, we find that all values observed experimentally are systematically wrong by a factor of between 1.5 and 2. The full lines in Fig. 10 show the values of τ calculated from the values of α obtained by the theory and multiplied by a fitting factor f_c, which is 2 at T = 10°C and 1.5 at T = 20°C.

Fig. 11 shows the corresponding results for $P_{CO_2} = 3 \cdot 10^{-4}$ atm. at 10° and 20°C. The fitting factor required for scaling the theory to the experimental results is 2 for both cases.

Finally, we have measured the time constants τ on natural pure limestone (Sollnhofen, F.R.G.) and on a cleavage surface of a $CaCO_3$ single crystal. The data points are given in Fig. 10 and fit well into those measured from marble. Even though the surface-controlled chemical rates might be different, the total dissolution rates are unaffected in laminar flow. At small $\delta \leqslant 5 \cdot 10^{-3}$ cm the

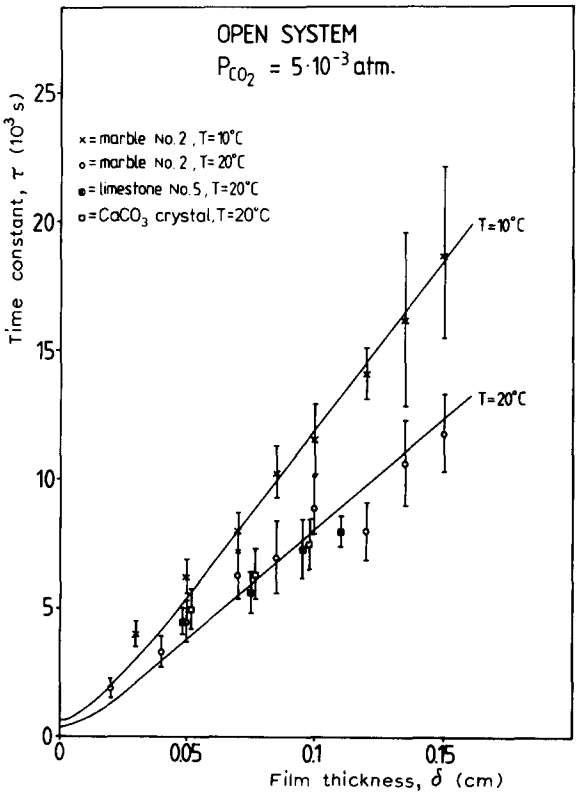

Fig. 10. Time constants of $CaCO_3$ dissolution measured for various film thicknesses at $P_{CO_2} = 5 \cdot 10^{-3}$ atm. and T = 10°C and T = 20°C. For T = 20°C measurements on limestone and a pure calcite crystal are included. The *solid lines* are the theoretical curves, fitted to the experiments by a factor f_c (see text).

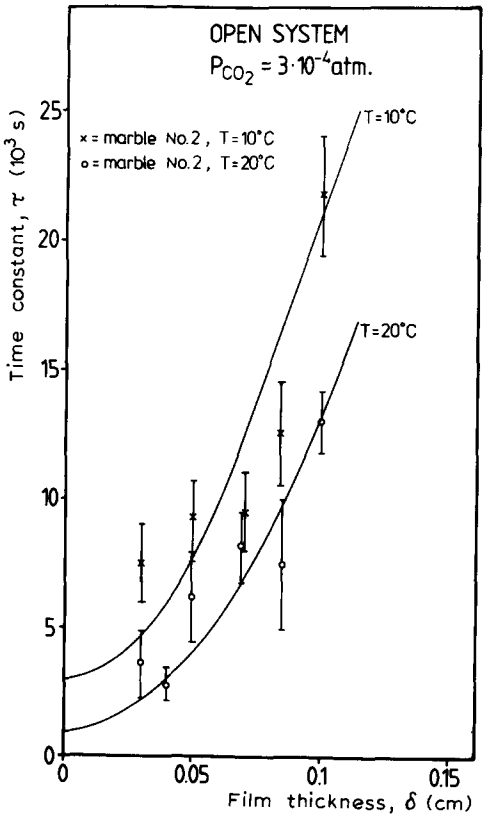

Fig. 11. Time constants of $CaCO_3$ dissolution measured for various film thicknesses at $P_{CO_2} = 3 \cdot 10^{-4}$ atm. and T = 10°C and T = 20°C. The *solid lines* are the theoretical curves, fitted to the experiments by a factor f_c (see text).

total rate is controlled entirely by CO_2 conversion and changes of the chemically controlled processes do not vary the rates. In the region for $\delta > 5 \cdot 10^{-3}$ cm diffusion is the slowest process. We have calculated in both cases the variation of the total dissolution rates, by changing all κ_i-values in the PWP equation (2) by a common factor between 0.5 and 2. In all cases the total dissolution rates do not change by more than 10%. This shows that at least for pure-limestone specimens our theory is well applicable in the region of laminar flow.

The fact that the experimentally observed time constants are larger by roughly a factor of 2 than theoretically predicted is not clearly understood and will be discussed in Section 4. Nevertheless the dependence of τ on temperature, P_{CO_2} and film thickness is in good agreement with that predicted from the theory. For geological applications the deviation by a factor of 2 does not seem of significant importance since in any case only an order of magnitudes can be given for the scales of geological processes.

The theoretical results show that in the case of turbulent flow, where the molecular diffusion coefficients have to be replaced by a much higher effective diffusion coefficient, D_{eff}, a steep increase in the dissolution rates occurs. We have therefore performed experiments for turbulent flow by stirred solutions, with thicknesses in the range 0.5 cm $\leqslant \delta \leqslant$ 1 cm. To do this, samples of marble were cut into circular discs of 5-cm diameter. They were surrounded by a rim of Teflon®, and water of known volume was put into the vessel so formed. The solution was stirred with a glass propeller. The measurements were performed in the way already described.

Fig. 12 shows the results for $P_{CO_2} = 3 \cdot 10^{-4}$ atm. and $P_{CO_2} = 5 \cdot 10^{-3}$ atm., at $T = 20°C$. To compare these results to the theory, we have to know the magnitude of D_{eff}, the effective diffusion coefficient that occurs in our experiment. This magnitude was determined experimentally in the following way. Instead of a $CaCO_3$ disc a disc of the same diameter was cut from a single crystal of KCl.

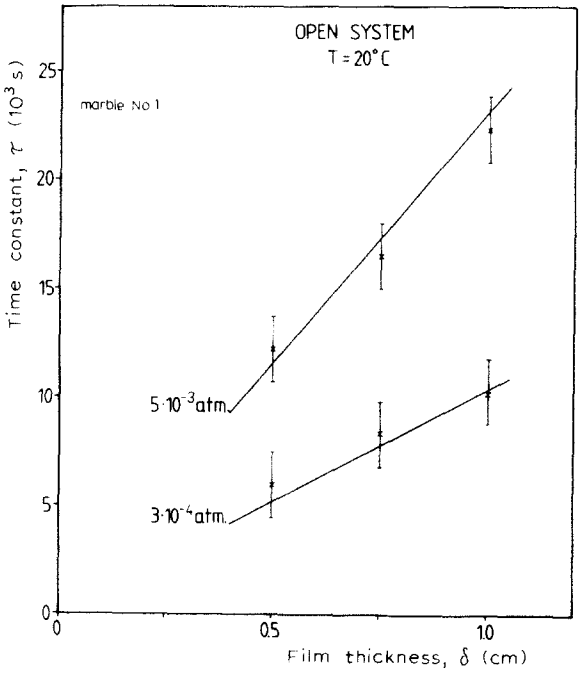

Fig. 12. Time constants of $CaCO_3$ dissolution measured under turbulent flow conditions for various film thicknesses and CO_2 pressures at $T = 20°C$. The speed of rotation of the glass stirrer is 200 r.p.m., which gives an effective diffusion coefficient, $D_{\text{eff}} = 1000 \cdot D_{CO_2}$. The *solid lines* are calculated with this value of D_{eff} and fitted to the experiments by a factor $f_c = 2.5$.

KCl dissolves readily in H_2O and we can assume that for KCl the surface-controlled dissolution rates are so large that the effective dissolution rates are determined only by diffusion. Furthermore the diffusion coefficients of K^+ and Cl^- are of the same magnitude as those of Ca^{2+}, CO_3^{2-}, HCO_3^-, etc. If the solution is stagnant on the KCl surface, we may assume that at the surface the solution is saturated and diffusion affects the mass transport. Thus, at any place in the solution the time dependence of the concentration of K^+ (or Cl^-) is given (Carslaw and Jaeger, 1959) by:

$$[K^+](t) = [K^+]_{eq}[1 - \exp(-t/T)] \qquad (39)$$

where

$$T = 4\delta^2/D_{K^+}\pi^2$$

For K^+ diffusion in a stagnant water film of defined δ the time constant is $T = 5 \cdot 10^4$ s

for $\delta = 1$ cm. The effective diffusion coefficient D_{eff} in the experiments with stirred solution is now determined in the following way. Water is put carefully to the KCl surface to a height of 1 cm. Two small Pt-electrodes are inserted into the water and the current at 0.5 V with a frequency of 1000 s^{-1} is measured. When the solution is now stirred the current increases rapidly in time. From the exponential behaviour of the current the time constant T_s is calculated. D_{eff} is determined from:

$$D_{eff} = D_{K^+} \frac{T}{T_S}$$

This was done for various stirring rates. Values of up to $D_{eff} \approx 10^3 D$ were obtained. These values were used mostly in our theory to calculate the dissolution rates for $CaCO_3$ under turbulent flow conditions.

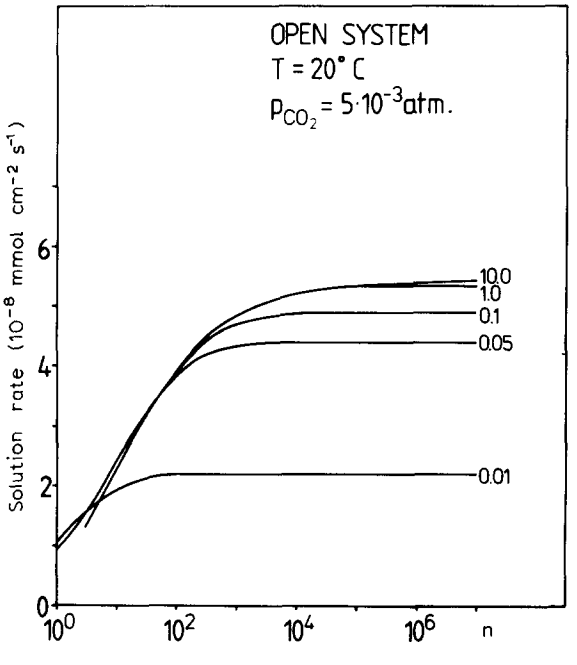

Fig. 13. Theoretical solution rates under turbulent flow conditions. The *number on the curves* gives δ in cm. The diffusion coefficient D_{CO_2} is multiplied by the factor n (*horizontal axis*) to give the effective diffusion coefficient D_{eff} for the calculations. At $\delta \geq 1$ cm the factor n must be greater than 10^4 to achieve maximum dissolution rates, i.e. fully developed turbulence.

Fig. 13 shows the dissolution rate for a $CaCO_3$ solution of $[Ca^{2+}] = 10^{-3}$ mmol cm^{-3} at $T = 20°C$ and $P_{CO_2} = 5 \cdot 10^{-3}$ atm. as a function of $D_{eff} = nD_{CO_2}$ for various δ. Increasing n shows increasing dissolution rates for all δ approaching constant rates for $n > 10^4$. In this region mass transport is governed by surface-controlled dissolution.

We have adjusted our stirring rate to obtain values of $n = 10^3$ and with this performed the measurements shown in Fig. 12. As in the case of stagnant films the time constants τ are too large by a factor of 2.5. The predicted hydraulic jump in the dissolution rates, when going from stagnant films to turbulent flow, however, is well observed. Depending on the Ca^{2+} concentration and on CO_2 pressure the dissolution rates increase by roughly one order of magnitude.

To summarize our experimental data we have plotted in Fig. 14 for $T = 20°C$ and $P_{CO_2} = 5 \cdot 10^{-3}$ atm. the dissolution rates predicted from the theory (full lines) and those derived from our experiments (dashed curves):

$$F = \alpha([Ca^{2+}]_{eq} - [Ca^{2+}]_{av}) \qquad (40)$$

where

$$\alpha = \delta / \tau$$

The experimental curves were fitted to the theory by use of a scaling factor of 0.4. The comparison shows that, apart from the scaling factor, the results are consistently well described by our calculations.

Finally, we have performed experiments for $CaCO_3$ deposition onto calcite surfaces. These experiments were performed by dropping a supersaturated solution onto a surface of calcite. For this purpose saturated solutions at P_{CO_2} of 1, 0.3 and 0.05 atm. were prepared by bubbling an atmosphere of known CO_2 content through double-distilled water and adding $CaCO_3$, reagent grade. The solution was stirred until saturation, measured by a pH electrode, was reached. After equilibrium was established the stirring rate was reduced, so that the excess $CaCO_3$ particles settled down on the bottom of the glass

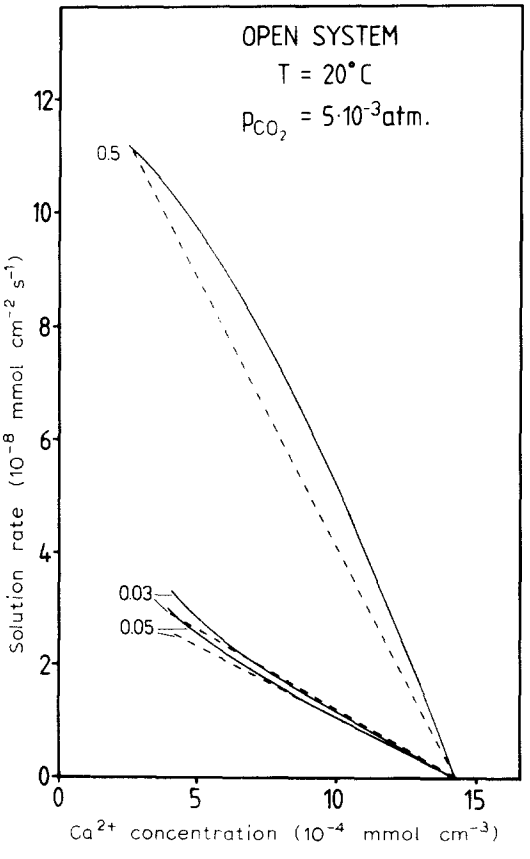

Fig. 14. Comparison of theoretical and experimental solution rates. The *dashed curves* are derived from the experiments by a fitting factor f_c, while the *full curves* represent calculations. The two upper curves represent turbulent flow conditions, the calculation being done with $D_{eff} = 10^3 D_{CO_2}$ as derived from the KCl experiment (see text). The *number on the curves* gives δ in cm.

vessel. The saturated solution was then pumped by a peristaltic pump at a rate of 0.6 ml min.$^{-1}$ and dropped to the surface of the calcite specimen.

The $CaCO_3$ samples were cut from a speleothem, the surface area was ~ 1 X 1 cm^2. These samples were embedded in plastic. After this the surface was ground and polished together with the plastic. By this procedure a large even surface was obtained in which the $CaCO_3$ sample was embedded. In this way we achieved an even distribution of the water film over the sample. The thickness of the film was determined by a method used by Dreybrodt (1980) and was 0.01 cm. This is the value which determines the growth rate of stalagmites.

The dripping rate to the surface was ~ 3 drops/min. To establish equilibirum of the solution supersaturated with CO_2 with respect to the surrounding atmosphere of $3 \cdot 10^{-4}$ atm. a time of ~ 9 s is needed (Dreybrodt, 1980). In the same time the quasi-stationary equilibrium (see Section 2.2) during the deposition is reached. Thus, during a time of ~ 10 s deposition takes place until the next drop brings new solution to the surface. During this time the Ca^{2+} concentration is practically unchanged and thus the deposition rate is constant.

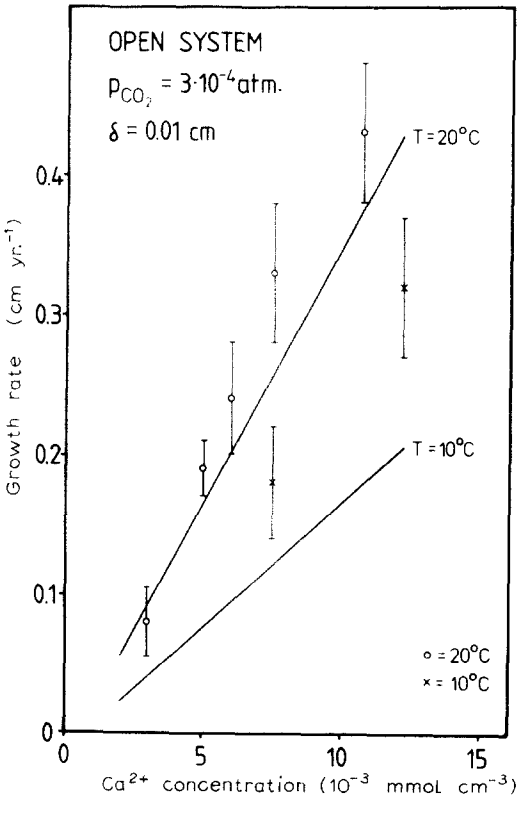

Fig. 15. Experimental growth rates of $CaCO_3$ at T = 10°C and T = 20°C. The initial Ca^{2+} concentrations are given on the *horizontal axis*. The CO_2 pressure of the surrounding atmosphere is $3 \cdot 10^{-4}$ atm. The *solid lines* are calculated with δ = 0.01 cm and $P_{CO_2} = 3 \cdot 10^{-4}$ atm.

The $CaCO_3$ specimens were left in place for a few days. After this they were weighed and the deposition rate was determined from the increase in weight. Fig. 15 shows the theoretical curves of the deposition rates together with the measured values. Within the limits already discussed the agreement is good. In contrast to the dissolution experiments no fitting factor f_c is needed.

One comment should be given here. Our theory can readily be applied to the growth of cave sinter. This problem has been treated by us in two publications (Dreybrodt, 1980, 1981c). In these papers the diffusion processes were taken into account only in part and the slow conversion of $H_2CO_3^0 \rightarrow CO_2$ was neglected. From the work reported here we can derive the growth rate at high drop rates

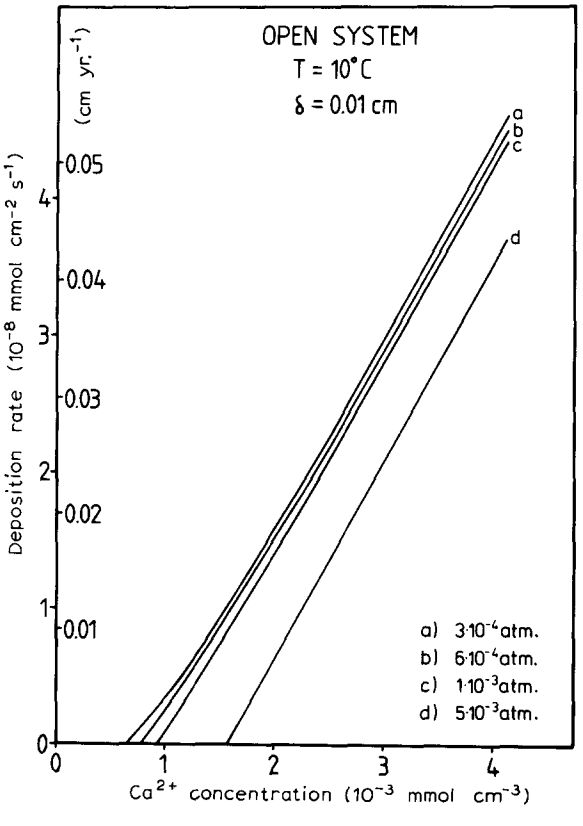

Fig. 16. Theoretical deposition rates of $CaCO_3$ at various CO_2 pressures of the surrounding atmosphere for geologically relevant initial Ca^{2+} concentrations.

(> 1 drop/min.) by directly applying our calculations.

Finally, Fig. 16 shows the results for $\delta = 0.01$ cm for various pressures of CO_2 commonly occurring in cave atmospheres and for Ca^{2+} concentrations of natural cave waters dripping onto stalagmites. We see immediately that in the range of P_{CO_2} between $3 \cdot 10^{-4}$ and $1 \cdot 10^3$ atm. the growth rates, calculated from the deposition rates (Dreybrodt, 1980), are practically independent of the cave atmosphere. There is, however, a strong temperature dependence, as one can see from Fig. 6. Furthermore the growth rate does not depend critically on the thickness of the water layer on top of the stalagmites, in contrast to our earlier calculations. The slow conversion of $H_2CO_3^0 \rightarrow CO_2$, which is now built into the theory reduces the growth rates in comparison to our earlier results.

4. Conclusion

We have developed a general theory of dissolution and deposition of $CaCO_3$ for the case of water films open to an atmosphere containing CO_2. The theory treats simultaneously the three rate-determining processes: surface-controlled dissolution or deposition at the calcite surface, diffusion of the molecular and ionic species in the solution, and slow conversion of $CO_2 \rightleftharpoons H_2CO_3^0$. Experiments have been carried out to compare experimental data to the theory. All the experiments show an agreement with the overall behaviour of the theoretical curves. For the case of dissolution the predicted values of α in their dependence on temperature, CO_2 pressure and film thickness scale with a factor $f_c \approx \frac{1}{2}$ consistently to the value observed experimentally. Thus, the observed rates are slower by a factor of 2 than those predicted by theory. For the precipitation experiments theory and experiment are in good agreement and no scaling factor is needed. Uncertainties in experimentally observed rates up to a factor of 2 are not unusual in calcite (Reddy et al., 1981).

The reason for this behaviour is not yet clear. It might have its cause in inaccuracies of the kinetic constants of $CO_2 \rightleftharpoons H_2CO_3^0$ conversion. In the region of $\delta \leqslant 0.2$ cm these constants influence the dissolution and deposition rates by the factor $(k_{eff}/D_{CO_2})^{1/2}$ (eq. 30). From this we see that inaccuracies in D_{CO_2} have the same effect as those of the kinetic constants, whereas the constants of the surface-controlled effect do not sensitively influence the results. To obtain agreement between theory and experiment a change of $(k_{eff}/D_{CO_2})^{1/2}$ to half of its value is sufficient. The kinetic constants of CO_2 conversion have all been determined in pure H_2O—CO_2 solutions and the effect of $[Ca^{2+}]$ on these constants is unknown. For the case of turbulent flow, dissolution and deposition are entirely determined by surface-controlled processes. In this case inhibition by Mg^{2+} ions, which were present in all dissolution experiments ($[Mg^{2+}]/[Ca^{2+}] \approx 0.02$), could lower the dissolution rates. Detailed experiments would be necessary to clarify these questions.

Nevertheless, for geological applications, where up to now not even the order of magnitude of most processes can be predicted theoretically, our theory is applicable to all situations in which open-system conditions determine the processes. The case of processes in which laminar flow is important can be approximated by plug flow, with even velocity distribution over the water film. In this case the theory of stagnant films is applicable. Although the exact inclusion of laminar flow changes the dissolution rates (Dreybrodt, 1980), the right order of magnitude is still obtained by our theory, which would become mathematically untreatable if those effects by laminar flow were included. The case of turbulent flow can be readily simulated by our theory of stagnant films by increasing the diffusion coefficients.

One very important result of our theory is the prediction of the hydraulic jump, which increases all dissolution and deposition rates by one oreder of magnitude once turbulent flow has commenced in films of sufficient thickness. This is of utmost importance in explaining the variety of different morphologies in the deposition of calcite in caves and the morphology of grykes and canons.

Furthermore our results can be applied to the problems of karst denudation. We will not discuss these problems here further, but will treat these in a later paper.

By changing the boundary conditions of the differential equations (5) solutions for closed-system conditions, which are important for applications in cave genesis and calcite deposition in joints, can be obtained. At present we are doing experiments and calculations for this case. The results will be published soon in a later paper (Buhmann and Dreybrodt, 1985).

Our results in Table II can be used by the geologist to get information on the dissolution rates in most important problems, which will be of utmost utility, since they provide information on plausible time scales. Of course our theory might be criticized since it does not include the effect of other ions, such as SO_4^{2-}, Cl^-, Na^+, Mg^{2+}, etc., which are always present in natural waters. First estimates of the effect of those ions show that the dissolution rates will not change drastically. However, experiments have to be performed for natural waters, to see whether this is true. This will be one of the future tasks.

In summary we feel that our theory is well applicable to geological situations in karst landforms and gives useful information to geologists working in this field.

Acknowledgements

The authors thank the Deutsche Forschungsgemeinschaft for financial support (Schwerpunktprogramm: "Hydrogeochemische Vorgänge im Wasserkreislauf in der ungesättigten und gesättigten Zone"). We wish to thank Dr. S. Kempe for stimulating discussions and Mr. G. Ankele for technical assistance in planning and setting up the experiments.

References

Bird, R.B., Stewart, W.E. and Lightfoot, E.N., 1960. Transport Phenomena. Wiley, New York, N.Y.

Buhmann, D. and Dreybrodt, W., 1985. The kinetics of calcite dissolution and precipitation in geologically relevant situations of karst areas, 2. Closed system. Chem. Geol. (submitted).

Carslaw, H.S. and Jaeger, J.C., 1959. Conduction of Heat in Solids. Oxford at the Clarendon Press, London, 2nd ed.

Cess, R.D. and Shaffer, E.C., 1959. Heat transfer to laminar flow between parallel plates with a prescribed wall flux. Appl. Sci. Res., Sect. A, 8: 339—344.

Curl, R.L., 1968. Solution kinetics of calcite. Proc. 4th Int. Congr. Speleol., 3: 61—66.

Dreybrodt, W., 1980. Deposition of calcite from thin films of natural calcareous solutions and the growth of speleothems. Chem. Geol., 29: 89—105.

Dreybrodt, W., 1981a. Kinetics of the dissolution of calcite and its application to karstification. Chem. Geol., 31: 245—269.

Dreybrodt, W., 1981b. Mixing corrosion in $CaCO_3$—CO_2—H_2O systems and its role in the karstification of limestone areas. Chem. Geol., 32: 221—236.

Dreybrodt, W., 1981c. The kinetics of calcite precipitation from thin films of calcareous solutions and the growth of speleothems: revisited. Chem. Geol., 32: 237—245.

Dreybrodt, W., 1982. A possible mechanism for growth of calcite speleothems without participation of biogenic carbon dioxide. Earth Planet. Sci. Lett., 58: 293—299.

Harned, H.S. and Hamer, W.J., 1933. The ionization constant of water. J. Am. Chem. Soc., 55: 2194—2206.

Hoover, T.E. and Berkshire, D.C., 1969. Effects of hydration on carbon dioxide exchange across an air—water interface. J. Geophys. Res., 74: 456—464.

Kamke, E., 1967. Differentialgleichungen. Akademische Verlagsgesellschaft Geest & Portig, Leipzig.

Kern, M.D., 1960. The hydration of carbon dioxide. J. Chem. Educ., 37: 14—23.

Landolt-Börnstein, 1969. Zahlenwerte und Funktionen aus Physik, Chemie, Astronomie, Geophysik und Technik, 6. Auflage, 5. Teil, Band (a). Springer, Berlin.

Picknett, R.G., Bray, L.G. and Stenner, R.D., 1976. The chemistry of cave waters. In: T.D. Ford and C.H.D. Cullingford (Editors), The Science of Speleology. Academic Press, London, pp. 213—266.

Plummer, L.N. and Busenberg, E., 1982. The solubilities of calcite, aragonite and vaterite in CO_2—H_2O solutions between 0 and 90°C, and an evaluation of the aqueous model for the system $CaCO_3$—CO_2—H_2O. Geochim. Cosmochim. Acta, 46: 1011—1040.

Plummer, L.N., Wigley, T.M.L. and Parkhurst, D.L., 1978. The kinetics of calcite dissolution in CO_2—water systems at 5°C to 60°C and 0.0 to 1.0 atm. CO_2. Am. J. Sci., 278: 179—216.

Plummer, L.N., Parkhurst, D.L. and Wigley, T.M.L., 1979. Critical review of the kinetics of calcite dissolution and precipitation. In: E.A. Jenne (Editor), Chemical Modeling in Aqueous Systems. Am. Chem. Soc., Symp. Ser., 93: 537—573.

Quinn, J.A. and Otto, N.C., 1971. Carbon dioxide exchange of the air—sea interface: flux augmentation by chemical reaction. J. Geophys. Res., 76: 1539—1549.

Reddy, M.M., Plummer, L.N. and Busenberg, E., 1981. Crystal growth of calcite from calcium bicarbonate solutions at constant P_{CO_2} and 25°C: a test of a calcite dissolution model. Geochim. Cosmochim. Acta, 45: 1281—1289.

Rickard, D. and Sjöberg, E.L., 1983. Mixed kinetic control of calcite dissolution rates. Am. J. Sci., 283: 815—830.

Skelland, A.H.P., 1974. Diffusional Mass Transport. Wiley, New York, N.Y.

Tien, C.L., 1959. On the eddy diffusivities for momentum and heat. Appl. Sci. Res., Sect. A, 8: 345—348.

Welch, M.J., Lifton, J.F. and Seck, J.A., 1969. Tracer studies with radioactive oxygen-15 — Exchange between carbon dioxide and water. J. Phys. Chem., 73: 3351—3356.

Weyl, P.K., 1958. Solution kinetics of calcite. J. Geol., 58: 163—176.

White, W.B. and Longyear, J., 1962. Some limitations on speleogenetic speculation imposed by the hydraulics of ground water flow in limestone. Nittany Grotto Newsl. (Natl. Speleol. Soc. U.S.A.), 10: 155—167.